Arabian Journal of Chemistry (2020) 13, 431–443

King Saud University

Arabian Journal of Chemistry

www.ksu.edu.sa
www.sciencedirect.com

ORIGINAL ARTICLE

Effect of synthesis pH on the physicochemical properties of a synthesized Bi_2WO_6 and the type of substrate chosen, in assessing its photo-catalytic activities

C. Jaramillo-Páez, J.A. Navío *, M.C. Hidalgo

Instituto de Ciencia de Materiales de Sevilla, Centro Mixto Universidad de Sevilla-CSIC, Américo Vespucio 49, 41092 Sevilla, Spain

Received 15 March 2017; accepted 20 May 2017
Available online 26 May 2017

KEYWORDS

Bismuth tungstate;
Photocatalysis;
Phenol;
Dyes;
Rhodamine B;
TiO_2(P25)

Abstract Crystalline orthorhombic Bi_2WO_6 powders were synthesized by a hydrothermal method from aqueous solutions of $Bi(NO_3)_3{\cdot}5H_2O$ and $Na_2WO_4{\cdot}2H_2O$ over a range of three selected pH values (2.0, 5.0 and 7.0), using NaOH as precipitating agent. The as-prepared catalysts were characterized by XRD, BET, FE-SEM, TEM, XPS and UV-vis spectroscopy. The effect of pH-synthesis on crystallinity, morphologies, surface area and optical absorption properties, were investigated. Although the pH has a marked influence on morphology, the nature of the precipitating agent (NaOH or TEA) also influences the morphology and surface structure composition, as it is observed in the present work. Three different probe molecules were used to evaluate the photo-catalytic properties under two illumination conditions (UV and Visible): Methyl Orange and Rhodamine B were chosen as dye substrates and Phenol as a transparent substrate. The photo-catalytic activities are strongly dependent not only on the pH used in the synthesis but also on the nature of the chosen substrate in assessing the photo-catalytic activities. Results were compared with those obtained when using TiO_2(P25, Evonik) in the same experimental conditions. The photo-catalytic activity of one of the synthesised samples has been evaluated by exposing a mixture of Rhodamine B and Phenol in water, to different illumination conditions. Our results provide new evidences about the issue of whether dyes are suitable substrates to assess the activity of a photo-catalyst.
© 2017 The Authors. Production and hosting by Elsevier B.V. on behalf of King Saud University. This is an open access article under the CC BY-NC-ND license (http://creativecommons.org/licenses/by-nc-nd/4.0/).

* Corresponding author.
E-mail address: navio@us.es (J.A. Navío).
Peer review under responsibility of King Saud University.

Production and hosting by Elsevier

1. Introduction

It is extensively recognized that TiO_2 is one of the most significance inorganic photo-catalytic materials (Nakata and Fujishima, 2012). However, the large band gap of TiO_2 (~3.2 eV for Anatase and Brookite, ~3.0 eV for Rutile) requires an excitation wavelength that falls in the UV region. Nonetheless, TiO_2 has proven to be useful material for

http://dx.doi.org/10.1016/j.arabjc.2017.05.014
1878-5352 © 2017 The Authors. Production and hosting by Elsevier B.V. on behalf of King Saud University.
This is an open access article under the CC BY-NC-ND license (http://creativecommons.org/licenses/by-nc-nd/4.0/).

environmental and disinfection applications (Abdel-Maksoud et al., 2016; Fagan et al., 2016; Malato et al., 2016). Therefore, it is desirable and urgent to develop highly efficient visible-light driven photo-catalysts for pollutant degradation. In principle, two approaches can be exploited to develop the visible-light-irradiation photo-catalysts: modification of TiO_2 and development of a novel material. The former has been largely investigated by doping different ions (Di Paola et al., 2012; Fagan et al., 2016; Mohamed et al., 2012; Shaham-Waldmann and Paz, 2016) to extend absorption wavelength range to visible region. Though a significant number of new photo-catalysts adequately perform under visible light, they typically display poor performance with respect to TiO_2 commercial references (e.g. Evonik P25) under sunlight. This has generated some controversy (Shaham-Waldmann and Paz, 2016) as to whether it is or not convenient, to move away from the use of TiO_2 and seek new alternatives in the field of synthesizing new photo-catalysts, operating in the visible region.

It is widely accepted that the use of visible light photons and the adequate overall handing of UV-vis radiation constitute the key point for a good photo-catalytic performance under sunlight illumination (Shaham-Waldmann and Paz, 2016). However, an increase in visible absorption, in principle, does not guarantee visible-light induced activity, since photo-catalytic reactions proceed by photo-generated charge carriers and poor photo-catalytic activity may be observed whether these charge carriers are highly recombined. Among others, bismuth-based materials and particularly Bi_2WO_6 seem to be suitable alternatives to widespread used TiO_2 (Colon et al., 2010; Yu et al., 2005). Bismuth Tungstate (Bi_2WO_6) is a typical n-type direct band gap semiconductor with a band gap of 2.8 eV and has prospective applications for the degradation of organic pollutants under visible light illumination due to its low valence band and high chemical stability (Hu et al., 2013). Considerable effort has been taken to synthesize these hierarchical photo-catalysts with small size so as to increase the separation rate of photo-induced charge carriers and consequently achieve high activities (Shang et al., 2008).

At the same times, it is widely accepted that the photo-catalytic performance of a catalyst is very closely related to its surface structure and crystallinity, including its morphology, crystallite sizes, specific surface area, crystal planes, defects, structure and composition of the surface and the synthesis pH values. All these factors, determine the result of the photo-catalytic activity that exhibits the photo-catalyst. Obviously, all these factors depend not only on the synthesis method, but also on the synthesis variables and pre- and post-treatment to the synthesis procedure. Thus, the photo-catalytic activity of Bi_2WO_6 prepared by solid state reaction in the leading works was relatively weak because of a small surface area of 0.64 $m^2\,g^{-1}$. Afterward, considerable progress has been achieved in the preparation of Bi_2WO_6 nanoparticles (Shang et al., 2008; Xu et al., 2009; Zhang and Zhu, 2005) and hierarchical superstructures with much increased surface areas and thus enhanced photo-catalytic behaviors.

Notably, Bi_2WO_6 has been prepared by a wide variety of synthesis methods, some of them are reported in a recent work (Wu et al., 2016). However, in most of these studies, Rhodamine B (RhB) and other dyes are used in the evaluation of photo-catalytic activity of the synthesized Bi_2WO_6 samples. RhB and other dyes are commonly used as model molecules, in part because their concentration can be easily monitored by UV-vis spectrometry. However, as pointed out by Yan et al. (2006) since dyes absorb light, especially in the visible range, the influence of this photo-absorption by dyes should be excluded for evaluation of the real photo-catalytic activity of the photo-catalysts. Also, as a remark, one should be careful when determining the dye concentration (for instance Methyl Orange, MO) during a photo-catalytic reaction because the pH may not be constant (acidic properties of the photo-degradation intermediates). Hence, the absorption spectra of a dye as MO may change (MO is a pH indicator!) which would cause error in the determination of the MO concentration.

In this study, Bi_2WO_6 was synthesized by following the same hydrothermal procedure which was described in our previous work (Murcia-López et al., 2013b) but varying the pH values of synthesis. Thus, samples that, once subjected to different calcination treatments, should have different physicochemical properties and therefore should also exhibit different photo-catalytic activities. Although there is some work on the effect of pH-synthesis on the morphology, structure or photo-catalytic activity of Bi_2WO_6 (Chunmei et al., 2009; Shang et al., 2008), however the effect of the pH-synthesis on the surface characteristics of Bi_2WO_6 has not been investigated. Regardless of this, the photo-catalytic properties of this material, obtained at different pH values, have been evaluated using RhB or other dyes, thus that the results of the photo-catalytic activities could be exalted.

The objective of this work was to synthesize Bi_2WO_6, through a hydrothermal route, to three pH values selected using NaOH (instead of TEA) as precipitating agent and to deepen not only on the structural and morphological characteristics of the obtained materials but also on the effects that the pH of synthesis exerts on the surface characteristics thereof.

At the same time, the aim was to use three different pollutants substrates, as probe molecules. For the photo-catalytic evaluation of the synthesized materials, we used two dyes: Rhodamine B (RhB) and Methyl Orange (MO) and a transparent substrate, Phenol (Ph). The obtained results provide important information about the choice of substrate for evaluation of photo-catalytic activity of the same material, in this case Bi_2WO_6, but having different physico-chemical properties. Results were compared with those obtained when using TiO_2(P25, Evonik) in the same experimental conditions.

2. Experimental details

2.1. Preparation of Bi_2WO_6

Bi_2WO_6 was prepared by following a hydrothermal procedure described elsewhere (Murcia-López et al., 2013b). In brief, about 0.01 mol of $Bi(NO_3)_3{\cdot}5H_2O$ was dissolved in 10 mL of glacial acetic acid, and the stoichiometric amount of the tungsten precursor (0.005 mol of $Na_2WO_4{\cdot}2H_2O$) was dissolved in 90 mL of distilled water. These two solutions were mixed forming a white suspension (pH ≈ 2), which was kept under stirring for 1 h. In another sequence preparations, the pH was adjusted to values of ca. 5 and 7 respectively by adding, drop wise to the suspension, a 2 M aqueous solution of NaOH (Panreac, > 98.0%). The obtained white suspensions, for each of the indicated pH values, were transferred independently into Teflon recipient inside a stainless steel autoclave. The hydrothermal treatment was done at 140 °C for 20 h, and then the precipitate was centrifuged, washed several times with portions of bidistilled water and dried overnight at 120 °C. Finally the samples were submitted to a calcination treatment at 300 °C for 4 h. The synthesized Bi_2WO_6 samples will hereafter be named as BW-x, where x is the pH of preparation. Commercial TiO_2(P25, Evonik) with anatase/rutile structure, was used as a reference photo-catalyst.

2.2. Characterization of the photo-catalysts

X-ray diffraction (XRD) patterns were obtained on a Siemens D-501 diffractometer with Ni filter and graphite monochromator using Cu Kα radiation $\lambda = 0.1541$ nm. Crystallite sizes were calculated from the line broadening of the main X-ray diffraction peak (1 3 1) of the Bi_2WO_6 russellite synthesized ($2\Theta = 28.3°$), with space group Pbca, using the Scherrer equation. Peaks were fitted using a Voigt function.

X-ray photoelectron spectroscopy (XPS) studies were carried out on a Leybold-Heraeus LHS-10 spectrometer, working

with constant pass energy of 50 eV. The spectrometer main chamber, working at a pressure $< 2 \times 10^{-9}$ Torr, is equipped with an EA-200 MCD hemispherical electron analyzer with a dual X-ray source working with Al Kα ($h\nu$ = 1486.6 eV) at 120 W and 30 mA. Bi $4f_{7/2}$ signal (159.6 eV) was used as internal energy reference in all the experiments. Samples were outgassed in the pre-chamber of the instrument at 150 °C up to a pressure $< 2 \times 10^{-8}$ Torr to remove chemisorbed water. All photoelectron spectra were analyzed using Casa-XPS software.

Light absorption properties of the samples were studied by UV–Vis spectroscopy. The Diffuse Reflectance UV–Vis Spectra (UV–Vis DRS) were recorded on a Varian spectrometer model Cary 100 equipped with an integrating sphere and using $BaSO_4$ as reference. Band gaps values were calculated from the corresponding Kubelka–Munk functions, F(R∞), which are proportional to the absorption of radiation, by plotting $(F(R\infty) \times h\nu)^{1/2}$ against hν.

The morphology for all the samples was analyzed by Field Scanning electron microscopy (FE-SEM) using a Hitachi S 4800 microscope. The samples were dispersed in ethanol using an ultrasonicator and dropped on a copper grid. Transmission electron microscopy (TEM) was performed in a Philips CM 200 microscope. The samples for the microscopic analyzes were dispersed in ethanol using an ultrasonicator and dropped on a carbon grid.

The porosity of the samples was characterized by measuring the N_2 adsorption isotherms at −196 °C in a volumetric analyzer (ASAP 2020, Micromeritics). Before the experiments, the samples were outgassed under vacuum (ca. 10^{-3} Torr) at 120 °C for 30 min in He flow. The isotherms were used to calculate the specific surface area, S_{BET} and total pore volume, V_{total}.

2.3. Photo-degradation tests

The photo-catalytic activity of the catalysts prepared was tested in the photo-assisted degradation of two chosen dyes: Methyl Orange and Rhodamine B and of a transparent substrate, the phenol. Methyl Orange, Phenol and Rhodamine B [Reagent Plus >99%] were supplied by Sigma-Aldrich. From this section we will use the abbreviations of the reagents used that will hereafter be named along the text as MO (Methyl Orange), as RhB (Rhodamine B) and as Ph (Phenol) occasionally.

Photo-catalytic tests were carried out using a discontinuous batch system, this includes a 250 mL Pyrex reactor enveloped by an aluminum foil, filled with an aqueous suspension (100 mL) containing the single substrates (concentrations: 20 ppm of MO, 50 ppm of Phenol or 10 ppm of RhB) and the photo-catalyst (1 g/L).

Two different illumination conditions were tested, using an Osram Ultra-Vitalux lamp (300 W) with a sun-like spectrum and a main line in the UVA range at 365 nm. The visible photo-catalytic experiments were performed using a polyester UV filter sheet (Edmund Optics) showing 99.9% of absorbance below 400 nm whereas under UV-conditions systems were illuminated through a UV-transparent Plexiglas® top window (threshold absorption at 250 nm).

The intensity of the incident UVA light on the solution was measured with a PMA 2200 UVA photometer (Solar Light Co.) being ca 90 W m^{-2} (UVA PMA2110 sensor; spectral response 320–400 nm).

On the other hand, the intensity of light in the visible range measured in this case was 110 W m^{-2} (Photopic PMA21300 sensor; spectral response 400–700 nm).

In order to favor the adsorption–desorption equilibrium, prior to illumination the suspension was magnetically stirred for 20 min in the dark. Magnetic stirring and a constant oxygen flow of 20 L/h, as an oxidant, were used to produce a homogeneous suspension of the photo-catalyst in the solution. A tank bubbler was used as a source of natural oxygen. All photo-catalytic tests started at pH ca. 5.5 and the total reaction time was 120 min.

During the Methyl Orange and Rhodamine B photoreactions, samples were collected at different times and in order to evaluate the dye discoloration rate, the concentrations of MO and RhB during the photo-degradation reactions were analyzed by UV–Visible spectroscopy, considering the main peak of each dye in the visible range, located at 465 nm (for MO) and 554 nm (for RhB). For this analysis a UV–Vis spectrometry with a Cary 100 (Varian) spectrometer was used. Phenol concentrations were followed using HPLC (Agilent Technologies, 1200 Series) equipped with UV-vis detector using an Eclipse XDB-C18 column (5 μm, 4.6 mm × 150 mm; Agilent) at 40 °C. Samples of about 2 mL were removed periodically during the experiments and filtered (Millipore Millex 25 0.45 mm membrane filter) previous to HPLC measurements. Mobile phase was water/methanol (65:35) at a flow rate of 0.8 mL/min.

On the other hand, following the recommendations of Ohtani (2014), we have proven that the initial concentrations of the substrates do not suffer variations, either under direct photolysis (negligible) or in the single presence of the catalyst, except in the latter case, in which the variations of concentration are due to an adsorption process in the dark until equilibrium is reached before illumination. Reproducibility of the measurements was ensured by double testing of selected samples.

Total organic carbon was followed by means of a TOC analyzer Shimadzu 500. Mineralization degrees (%) were evaluated by the TOC values upon 2 h of illumination, for all the photo-assisted processes studied, using the formula [1 − (final TOC/initial TOC)] × 100.

3. Results and discussion

3.1. Characterization

Fig. 1 shows the XRD patterns of the photo-catalysts; the diffraction patterns of Bi_2WO_6 were well indexed to the russellite synthetic phase (JCPDS 39-0256, orthorhombic phase), constituted of a layered structure containing WO_6 octahedra and $(Bi_2O_2)^{2+}$ layers and H_2O molecules (Amano et al., 2009; Babu et al., 2014a, 2014b). No diffraction peaks were observed for the starting precipitate precursors obtained by simple inorganic precipitate reaction before hydrothermal treatment. Therefore, it can be concluded that the hydrothermal treatment is essential for the formation of crystalline Bi_2WO_6. Likewise, no other possible impurities, such as WO_3 or Bi_2O_3, were detected, indicating that the as-prepared Bi_2WO_6

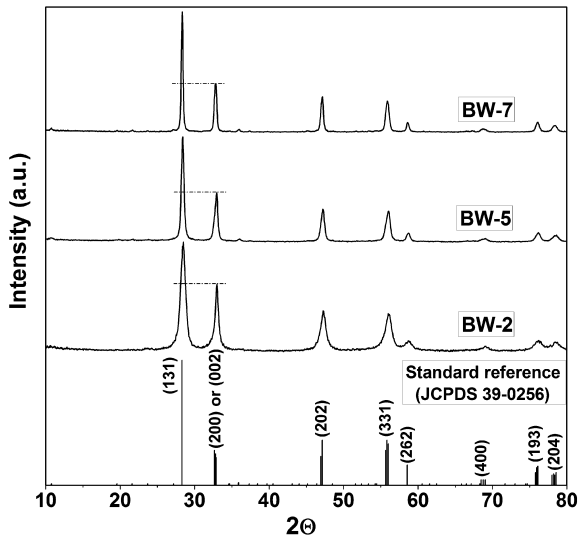

Figure 1 X-ray diffraction patterns of the prepared photocatalysts.

was pure. From Fig. 1 it can be clearly seen that increasing the pH of synthesis, the width of the diffraction peaks becomes gradually narrower, and thus indicating a better crystallinity. In fact, with the improvement of crystallization, the crystallite sizes grow larger as has been estimated according to the Scherrer equation, and the surface areas of the samples decrease (Table 1). Based on the standard data, the intensity of the (131) peak is approximately five times that of the (200) or (020). However, the intensity ratio of the (131) peak to the (200) or (020) peak in the as-prepared Bi_2WO_6 samples was less than 2.5. This fact reveals that the synthesized BW-x samples exhibited anisotropic grow in the (200) or (020) direction.

The XPS technique was used to identify the surface chemical composition and the oxidation state of the synthesized Bi_2WO_6 samples. Table 2 shows the results obtained by XPS of the elemental atomic quantification of the synthesized samples and Fig. 2 shows the surface features of the synthesized BW-x series. In none of the samples, the presence of sodium on the surface was detected. The two peaks into de Bi 4f region (Fig. 2A–C) at 164.8 eV and 159.6 eV can be attributed to Bi $4f_{5/2}$ and Bi $4f_{7/2}$ respectively (Jaramillo-Páez et al., 2017) and are characteristic of Bi^{3+}. The binding energies of 37.8 eV and 35.6 eV with a spin–orbital separation of 2.2 eV, as shown in Figs. 2 D, 2 E and 2 F, could be assigned to the +6 oxidation state of tungsten for the W $4f_{5/2}$ and $W_{7/2}$ respectively (Wang et al., 2013). The O 1s region (Fig. 3A–C) can be fitted using two peaks, which are consistent to different chemical environments of oxygen element in Bi—O and W—O bonds, the relative areas of which vary as the pH of synthesis changes. The XPS peaks in the O 1s at 529.4 eV and 530.2 eV are attributable to Bi—O and W—O bonds in the BW-x series respectively (Jaramillo-Páez et al., 2017; Wang et al., 2013). Table 2 also shows the percentages of the relative areas of the two oxygen peaks of the O 1s region of the XPS spectrum due to contribution Bi—O and W—O bonds in for each sample. Taking into account the relative contributions of the peaks assigned to O—W (530.2 eV) and O—Bi (529.4 eV) links, we have made estimations of the O/W and O/Bi ratios on the surfaces of each sample, establishing species cationic and anionic that are compatible with the oxidation states Bi (3+) and W (6+) in the stoichiometric Bi_2WO_6 at the surface. According to these estimates, the surface of each of the samples can be understood as formed by anionic and cationic species as follows: BW-2 ($[Bi_2O_2]^{2+}$ and $[WO_4]^{2-}$; BW-5 ($[Bi_2O_2]^{2+}$ and $[WO_4]^{2-}$; BW-7 ($[WO_2]^{2+}$ and $[Bi_2O_4]^{2-}$). Thus, the surface structure of the samples prepared at acidic pH values is consistent with a layer structure formed by octahedral species WO_6 and $[Bi_2O_2]^{2+}$ layers (Babu et al., 2014a; Ohtani, 2014) while the surface of the BW-7 samples should be understood in terms of $[WO_2]^{2+}$ and $[Bi_2O_4]^{2-}$ species. This result implies that at pH = 7, the Bi^{3+} and W^{6+} species have been rearranged on the surface of the BW-7 sample, differently than the BW-2 samples and BW-5, without any changes in the structure. In fact, the existence of WO_2^{2+} species is well established; thus, for example, WO_2Cl_2 is a layered material, consisting of distorted octahedral W centers (Abrahams et al., 1993; Bortoluzzi et al., 2016).

The effect of the pH during the synthetic procedure on the morphology of the as-obtained Bi_2WO_6 samples was investigated by FE-SEM. Fig. 4 shows selected SEM micrographs of the synthesized samples. Clearly, the morphologies and dimensions of the samples are strongly depending on the pH value. BW-2 showed 3D flower-like spherical superstructures (Fig. 4 A) with a diameter ranging between 5 and 8 μm constructed by sheets aligned perpendicularly to the spherical surface (Fig. 4B). Fig. 4 A further reveals that the flower-like superstructures were occasionally assembled by two-dimensional micrometer sheets (marked in Fig. 4A). However, for the Bi_2WO_6 samples synthesized at higher pH values (pH ca. 5.0 or 7.0) a sheet-like morphology was observed being heterogeneous in sizes, although the sample prepared at pH = 7.0 displays bigger sheet-sizes than the sample prepared at pH = 5.0, by comparing Fig. 4D and E. The thickness of the thin sheet-shapes was estimated at 0.04 μm (Fig. 4F).

The detailed morphology of the BW-x samples was further investigated with TEM. Fig. 5 shows the TEM photographs of BW-x samples. Fig. 5A shows that the structure of the sheets is grouped together following a circular tangential direction, which is in accordance with the SEM photographs (Fig. 4A). A large proportion of sheets can be seen in lateral position

Table 1 Some of the physicochemical properties of the synthesized BW-x samples.

Sample	Crystallite size (nm)	Band gap (eV)	S_{BET} ($m^2\ g^{-1}$)	Pore volume (cm^3/g nm)
BW-2	11.7	2.78	24.0	0.0032
BW-5	28.1	2.98	19.2	0.0027
BW-7	64.5	2.94	8.0	0.0018
TiO_2(P25)	–	3.20	43.8	0.0081

Table 2 Proposed of surface species based on XPS results for BW-x samples.

	Bi (4f) (atomic %)	W (4f) (atomic %)	O (1 s) (atomic %)	Contribution area (%)	Atomic ratio
BW-2	(26.95)	(9.87)	(63.17)	O—W (60.53)	O/W = 38.24/9.87 = 3.87 (≈4:1) $[WO_4]^{2-}$
				O—Bi (39.47)	O/Bi = 24.74/25.67 = 0.92 (≈1:1) $[Bi_2O_2]^{2+}$
BW-5	(25.62)	(9.04)	(65.34)	O—W (51.83)	O/W = 33.86/9.04 = 3.60 (≈ 4:1) $[WO_4]^{2-}$
				O—Bi (48.17)	O/Bi = 31.47/25.62 = 1.22 (≈1:1) $[Bi_2O_2]^{2+}$
BW-7	(26.09)	(9.57)	(64.33)	O—W (24.21)	O/W = 15.57/9.57 = 1.62 (≈2:1) $[WO_2]^{2+}$
				O—Bi (75.79)	O/Bi = 44.80/23.97 = 1.87 (≈2:1) $[Bi_2O_4]^{2-}$

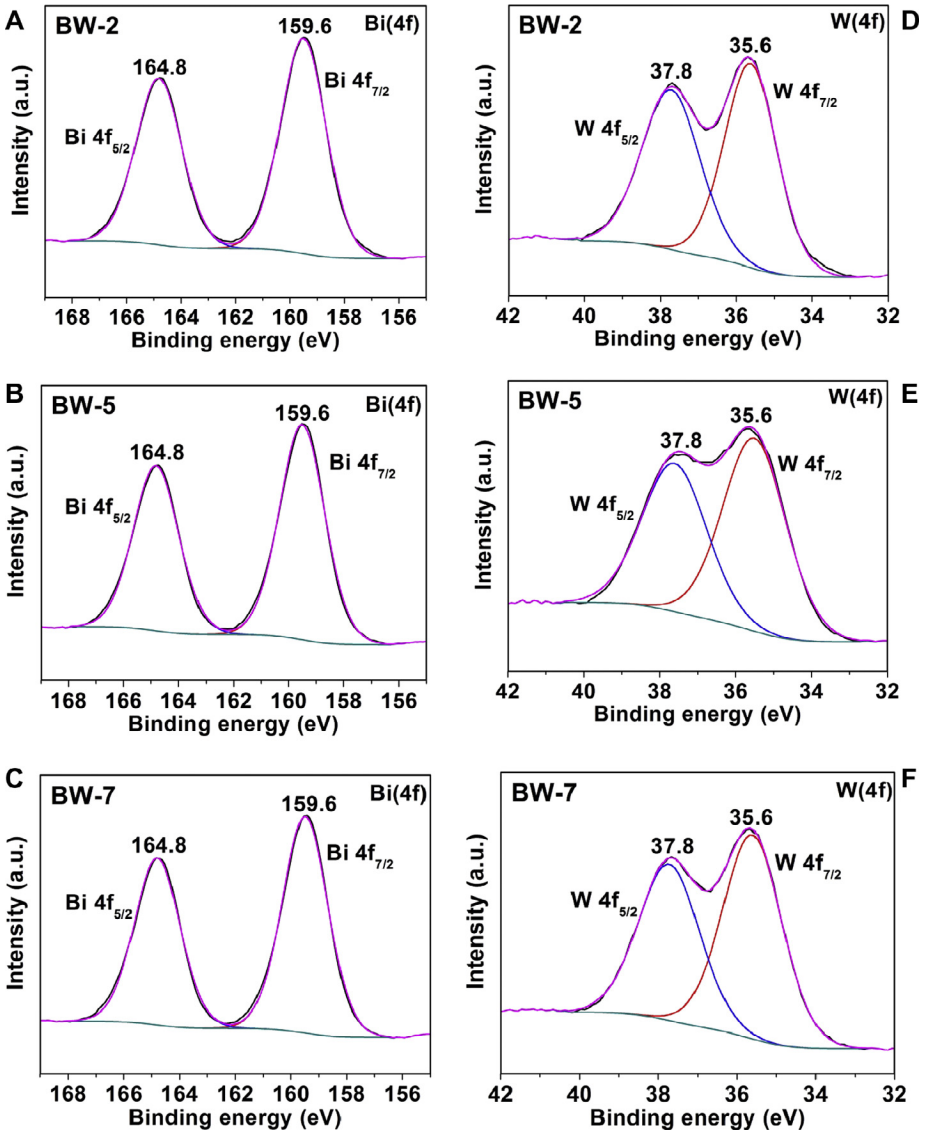

Figure 2 XPS results, in the Bi 4f and W 4f region of the synthesized BW-x samples.

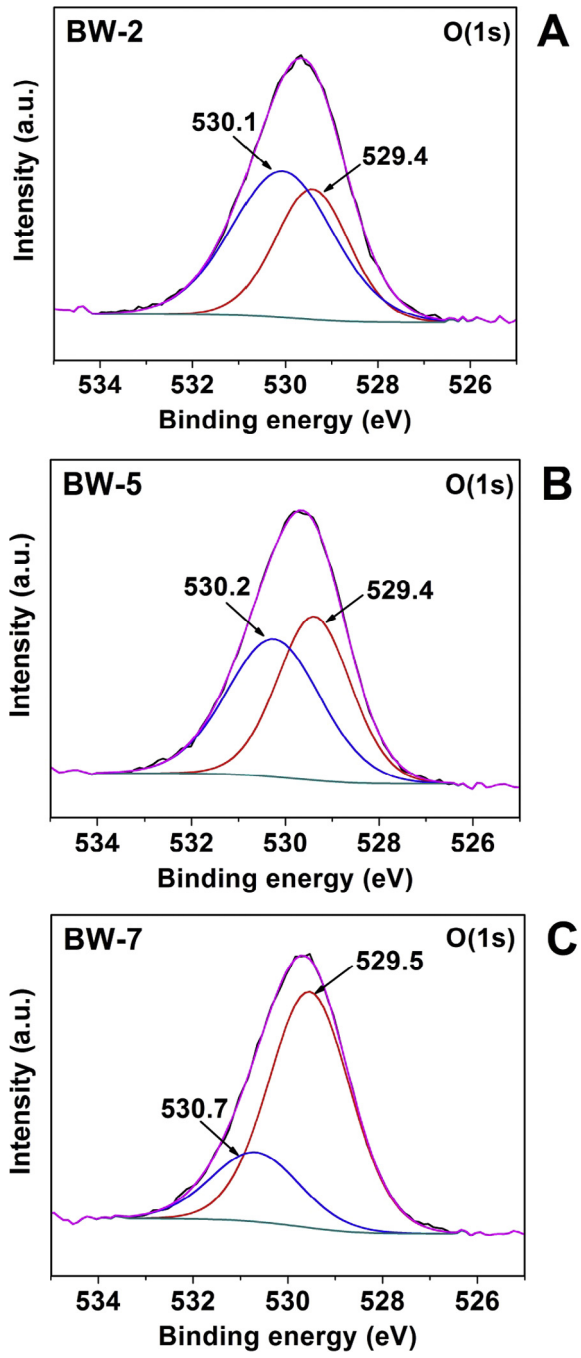

Figure 3 XPS results, in the O 1s region of the synthesized BW-x samples.

(indicated with arrows). However, it can be seen that BW-5 and BW-7 appear the square morphology with the size 50–200 nm. The corners and the surfaces of the BW-5 and BW-7 nanosheets are smooth.

In a previous work (Colon et al., 2010) we report the synthesis of Bi_2WO_6 following the same procedure but adjusting the pH by adding TEA (triethylamine). In that work, we also report that the morphology of the Bi_2WO_6 catalyst appears highly influenced by the precipitation pH. Thus, at low pH the particles show sheet-like morphology while by increasing the precipitation pH with TEA a regular 3D hierarchical superstructure is formed through an Ostwald ripening process (Amano et al., 2008; Zhang et al., 2007). However, in the present work, at low pH the particles show a tendency to flower-like superstructure, while by increasing the precipitation pH with NaOH the particles show a sheet-like morphology, at least until pH = 7.0. This result suggests that, regardless of the effect of pH, other factors such as the presence of either hydroxyls or surfactants in the synthesis medium can affect the morphology of the samples. In any case, it is evident that, from the results of characterization, the pH of synthesis of Bi_2WO_6 sample has an effect on the physico-chemical properties of the obtained samples (Table 1), which can influence on the photo-catalytic activity. On one hand, it can be seen (Table 1), from crystallite sizes, that the samples prepared at low pH are less crystalline than those obtained at a higher value, and this effect influences the values of specific surfaces areas, being higher for BW-2 relative to BW-7. The study and control of morphology has been extensively studied in Bi_2WO_6 photo-catalysts. The nanosheets growth mechanism of this compound in neutral pH conditions has been proposed by Zhang and Zhu (2005). Thus, a crystalline structure is formed from Bi_2WO_6 small amorphous particles, thanks to the typical hydrothermal process ripening in which small crystal nuclei are initially formed in the supersaturated middle. Because of the difference in solubility between small and large particles (according to the Gibbs-Thomson law), growth is favored at the first cost of the dissolution of the latter this tends to be anisotropic growth and parallel to WO_6 octahedra layer and has been explained as a consequence of the intrinsic structural characteristics of tungstates associated with the chemical potential of some faces on underlying distorted octahedral chains $[WO_4]^{2-}$ (Zhang and Zhu, 2005). However, using Pluronic P123 surfactant, it is possible to suppress the anisotropic growth and formation of nanosheets of Bi_2WO_6 (Zhang et al., 2011). Possibly, in our synthesis conditions, the NaOH (instead of TEA) is facilitating the formation of sheet-like morphology. The influence of pH on the synthesis of such structure materials has been explained through two effects: first, a relationship between the concentrations of ions in the system during the aging process, influencing the rate of one species over the other and, secondly, the possible formation of oxyanions $[WO_4]^{2-}$ or polyanions of other species due to the presence of hydroxyl OH^- ions. In any case, it is clear that there is a deep dependence of morphology with the method and conditions of preparation, even in the case of procedures performed by hydrothermal synthesis.

The optical properties of the samples were also explored by UV–Vis diffuse reflectance spectroscopy (Fig. 6). Commercial TiO_2(P25, Evonik) is also shown as reference. As can be seen, the synthesized Bi_2WO_6 samples as well as the commercial TiO_2(P25, Evonik), presents the photo-absorption property from the UV light region to visible light shorter than 450–475 nm corresponding to the band gap values reported in Table 1. The band edge of Bi_2WO_6 shift with different pH. As shown, the sample BW-2 has the lowest value of band gap, when compared with the values obtained for the other samples (Table 1). In fact, this sample presents a very pale yellow-green color, as opposed to the other samples which exhibit a whitish color. Self-assembled layered structure can cause multiple scattering of the light, which would increase optical path of light propagation through the layered structure. Multiple scattering of UV-vis light increases their light

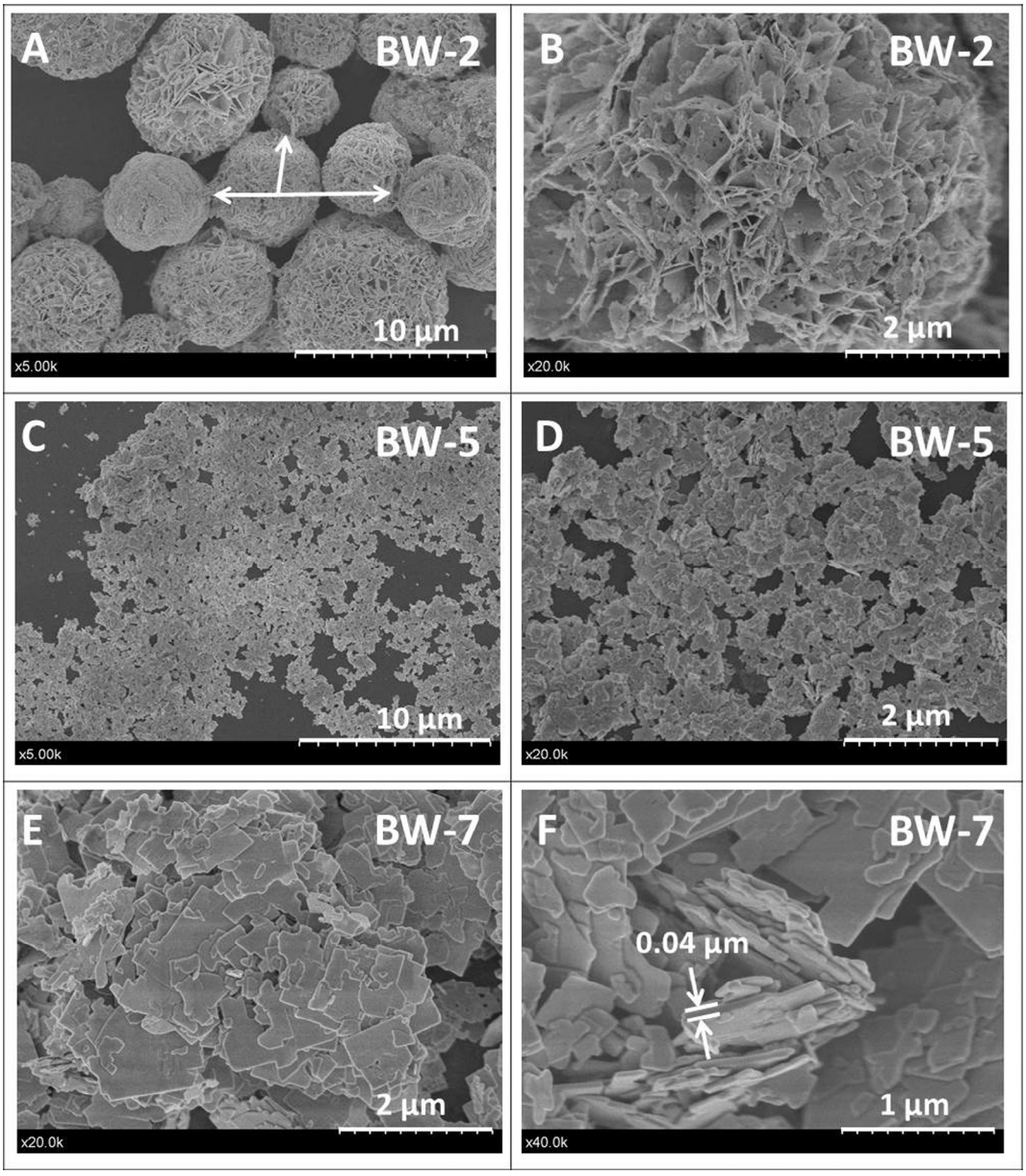

Figure 4 FE-SEM images of the as-prepared BW-x samples. (A) and (B) BW-2; (C) and (D) BW-5; (E) and (F) BW-7.

absorption and light utilization rate, resulting in a decrease in band gap. Accordingly it is found that the difference in morphology between the BW-2 sample and the other ones, BW-5 and BW-7, can do affect the optical absorption and band gap energy of the samples, as can be observed (Fig. 6).

Fig. 7 shows the evolution of pore diameter distributions for samples prepared in this study; TiO_2(P25, Evonik) is also shown as reference. As it can be observed, BW-x samples present a sharp pore family at about 2–3 nm (microporous) whose volume slightly decreases as the pH increases. These pores at about 2–3 nm are probably slits produced by sheets stacking. These results suggest that the pH of synthesis influences the texture of the samples as expected. On the other hand, the pore volume is bigger in TiO_2(P25, Evonik) than in BW-x samples. Moreover, BW-2 sample exhibited additional pore family at higher diameters, between 5 and 20 nm (mesoporous) that is more or less absent in samples BW-5 and BW-7, although BW-5 sample shows a broad distribution of pore size between 20 and 100 nm similar to that presented by TiO_2(P25, Evonik) in the same region. Mesoporous in BW-2 is likely caused by the flower structure according to Fig. 4A and B.

Although the pH of synthesis and the nature of the precipitating agent (NaOH or TEA) seem to have marked influence on the physicochemical properties of Bi_2WO_6, the nature of the substrate chosen to evaluate the photo-catalytic activity is another factor to consider when establishing the photocatalytic properties of a catalyst. In our studies, we have chosen three substrates of different nature, which they have been widely used in scientific literature due to its toxic nature.

3.2. Photo-catalytic experiments

The photo-catalytic activity of the as-obtained samples was evaluated by the degradation of Rhodamine B (RhB), Methyl

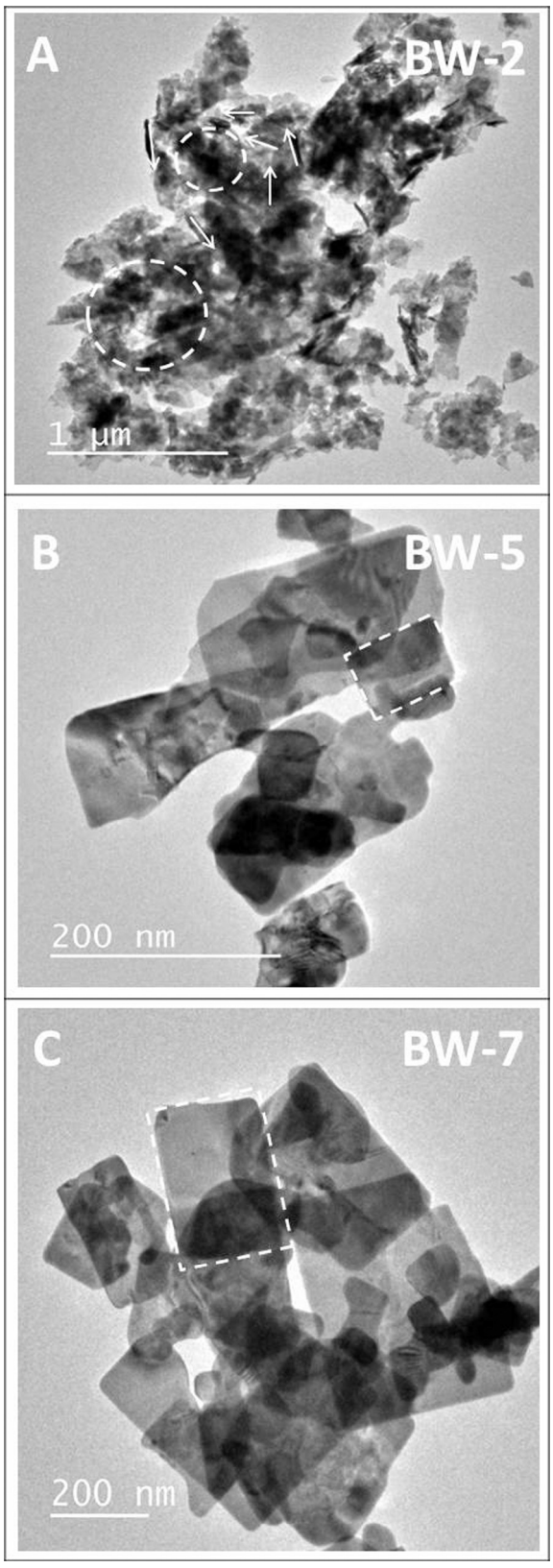

Figure 5 TEM images of the as-prepared BW-x samples. (A) BW-2, (B) BW-5 and (C) BW-7.

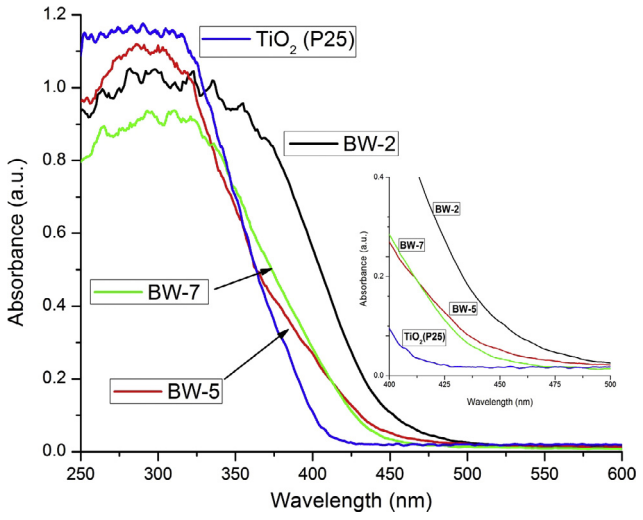

Figure 6 UV-vis diffuses reflectance spectra of the as-prepared samples and TiO_2(P25). A magnification in the region of 400–500 nm is shown (inset).

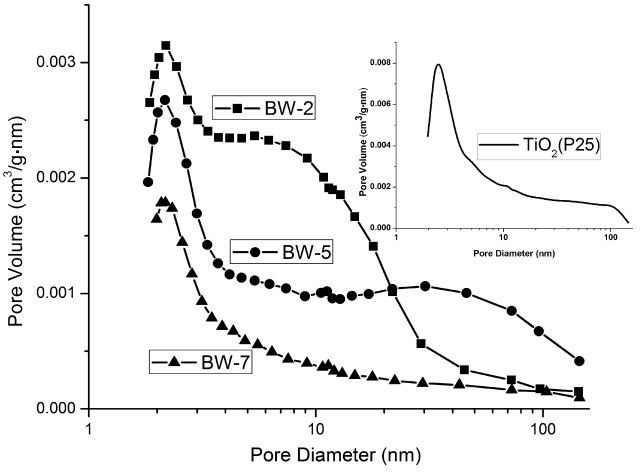

Figure 7 Pore diameter distributions of the studied materials.

Orange (MO) and Phenol (Ph) aqueous solutions under the experimental conditions indicated previously. Fig. 8 shows the conversion plots for photo-chemical discoloration of MO (Fig. 8A) and photo-chemical disappearance of Phenol (Fig. 8B) and RhB (Fig. 8C) under UV and Visible illumination using the synthesized Bi_2WO_6 samples. It is clear that the percentages of degradation depend not only on the nature of the substrate studied, but also on the pH of the catalyst synthesis and obviously on the illumination conditions. Thus, while the synthesized catalysts show low values of conversion for MO substrate, they however showed high conversion values when the RhB is used, being the values for Phenol conversion, moderate. The results also indicate that the synthesized catalysts showed better results under lighting conditions in the UV, than under visible illumination.

Fig. 9 shows the results of the conversion percentages of the three selected substrates, using the commercial TiO_2(P25, Evonik),

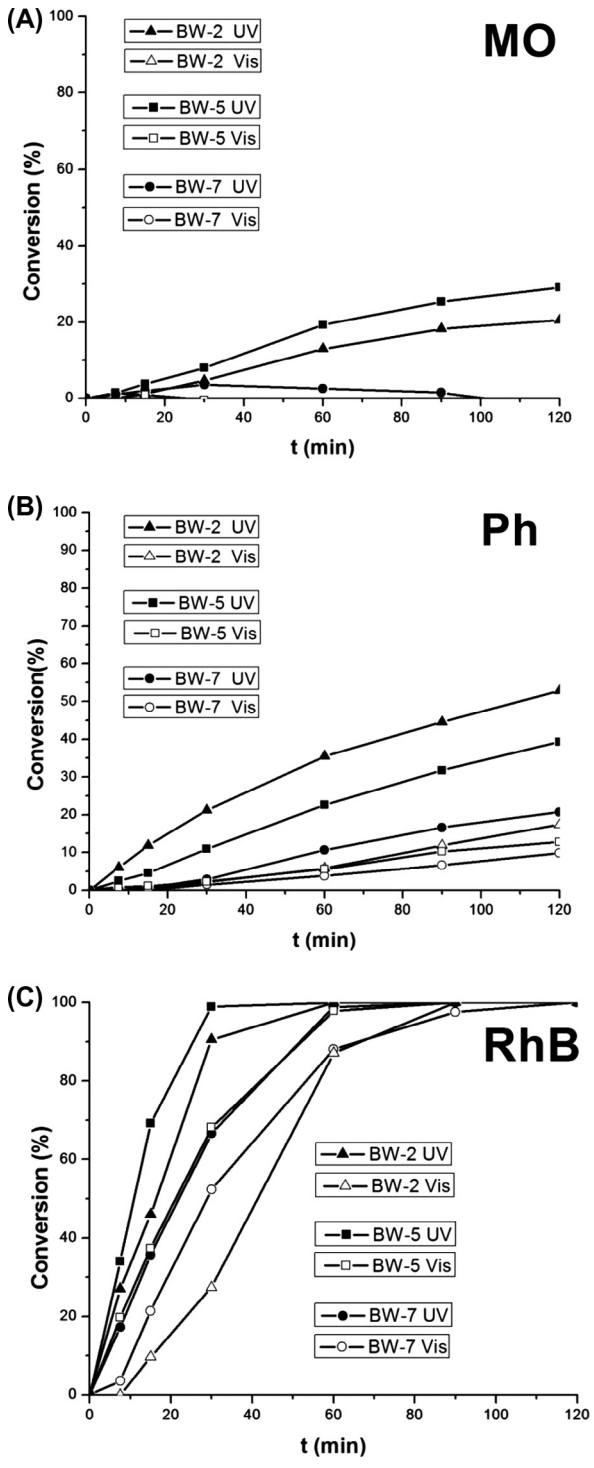

Figure 8 Conversion plots for photoassisted transformations of Methyl Orange (A), Phenol (B) and Rhodamine B (C) using the indicated BW-x catalyst under UV and visible illumination.

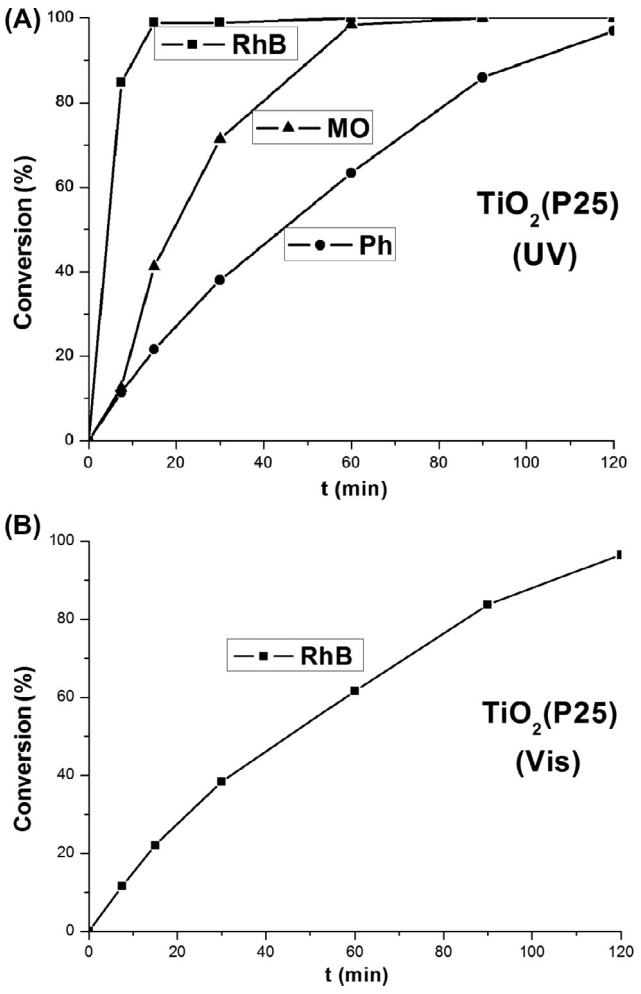

Figure 9 Conversion plots for photochemical discoloration of Methyl Orange (MO), Phenol (Ph) and Rhodamine B (RhB) disappearance, under (A) UV or (B) sun-like illumination: with only the presence of commercial TiO_2(P25) photo-catalyst.

under two illumination conditions. As can be seen (Fig. 9A), TiO_2(P25, Evonik) showed high values of conversion for three substrates, especially for RhB, under illumination in the UV. However, under Visible illumination (Fig. 9B), only conversions for RhB was obtained but not for Phenol or for MO. This last fact is not surprising, since according to our previous results (Abrahams et al., 1993; Colon et al., 2010), the TiO_2 (home-prepared) presented photo-catalytic activity in the visible, when Rhodamine B is used, due to added photo-sensitizing effect.

In order to compare the photo-catalytic activity of the synthesized samples and the commercial titania, in Fig. 10A the values of the initial reaction rates of degradation, under UV-illumination, of each of the substrates with the indicated catalysts and the values of the reaction rates per surface area unit (Fig. 10B) are shown. Similarly, Fig. 11 shows the values of reaction rates under lighting conditions in the visible. The reaction rates were calculated from the slopes of the conversion plots at the first 15 min of reaction, and assuming zero-order kinetics at this stage of the reaction.

The differences between the BW-x series could be attributed to structural (crystallinity), morphology and surface areas features. Crystallinity, morphology and the surface area of the photo-catalyst are two important factors influencing the photo-catalytic activity. The higher the crystalline quality, the smaller the amount of defects. The defects operate as trapping and recombination centers between photo-generated

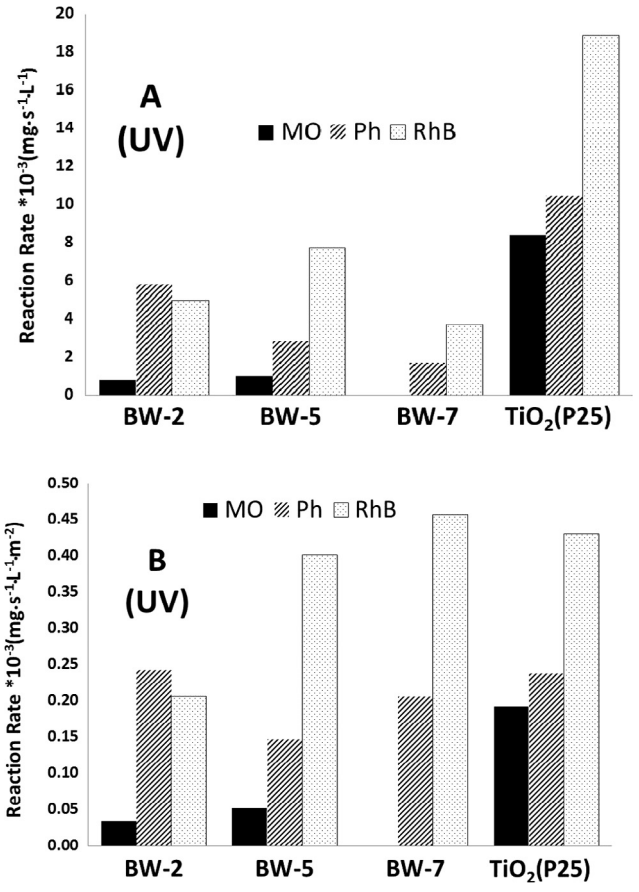

Figure 10 UV-photo-catalytic activity of Methyl Orange (MO), Phenol (Ph) and Rhodamine B (RhB) using the indicated photo-catalysts: (A) initial reaction rates and (B) initial reaction rates per surface area unit.

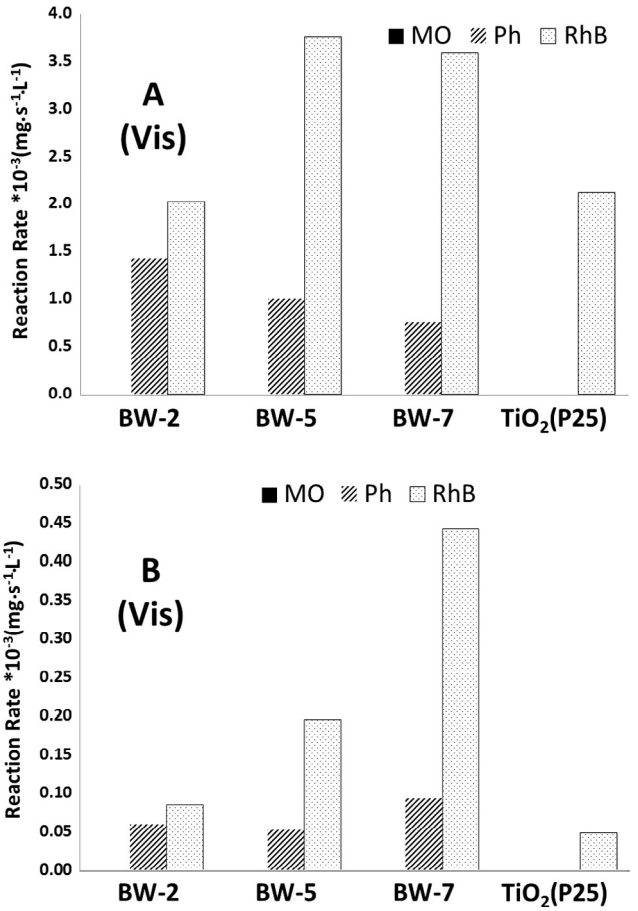

Figure 11 Sun-like photo-catalytic activity of Methyl Orange (MO), Phenol (Ph) and Rhodamine B (RhB) using the indicated photo-catalysts: (A) initial reaction rates and (B) initial reaction rates per surface area unit. The reaction rate of MO is not indicated because, under the experimental conditions it was close to zero.

electrons and holes, resulting in a decrease in the photo-catalytic activity. Therefore, a high degree of crystallinity is required for photo-catalysts. In this sense, BW-7 has the highest crystallinity (Fig. 1, Table 1) although the lowest surface area.

When comparing the initial reaction rates per surface area, for each substrate with the synthesized Bi_2WO_6 samples, it is observed that BW-7 is the most photo-active catalyst for RhB degradation (both in UV and in visible illumination), however, this same sample is the worst photo-catalysts studied, in the MO degradation (both in UV and in visible illumination). Even though TiO_2(P25, Evonik) seems to be more photo-active than BW-7 for RhB degradation under UV-illumination (Fig. 10A), when the initial rates are normalized by area, it becomes similarly photo-active than BW-7 (Fig. 10B). It is interesting to note that the BW-x synthesized catalysts were found to be active in the visible, at least for the degradation of phenol and RhB, showing under these lighting conditions (Fig. 10B), better results for the degradation of RhB, than those obtained with TiO_2(P25, Evonik).

From the results obtained, two important aspects should be highlighted: on one hand, comparison among the different materials and, on the other, influence of the selected model molecule.

Final mineralization degrees were calculated from the TOC measurements and these values are shown in Fig. 12. In the tests using the three BW-x synthesized catalysts and TiO_2(P25, Evonik) under UV and Vis illumination, the comparison of the mineralization degrees obtained with the MO, Phenol and RhB, indicates that TiO_2(P25, Evonik) under UV-illumination was the best catalyst, obtaining a high degree of mineralization for each one of the studied substrates. Irrespective of this fact, the catalysts synthesized showed good degree of mineralization in the UV, when tested with RhB. It is interesting to note, that evaluations of photo-catalytic activity of BW-x synthesized materials using the MO, lead to low (or zero) values of the initial reaction rates under both lighting conditions in the UV and Vis. (Figs. 10 and 11) and consequently to low percentages of mineralization or no mineralization was detected (Fig. 12). However, if Phenol is used as substrate model, it can be seen (Figs. 10 and 11) that, although the initial reaction rates are very similar, both in the UV and in the visible, for the three synthesized catalysts, the mineralization percentages are different; however, better rates of mineralization are obtained for the sample BW-2, both in the UV and in the visible (Fig. 12).

Given that one thing is the photo-catalytic activity measured using a given substrate as test molecule, and another

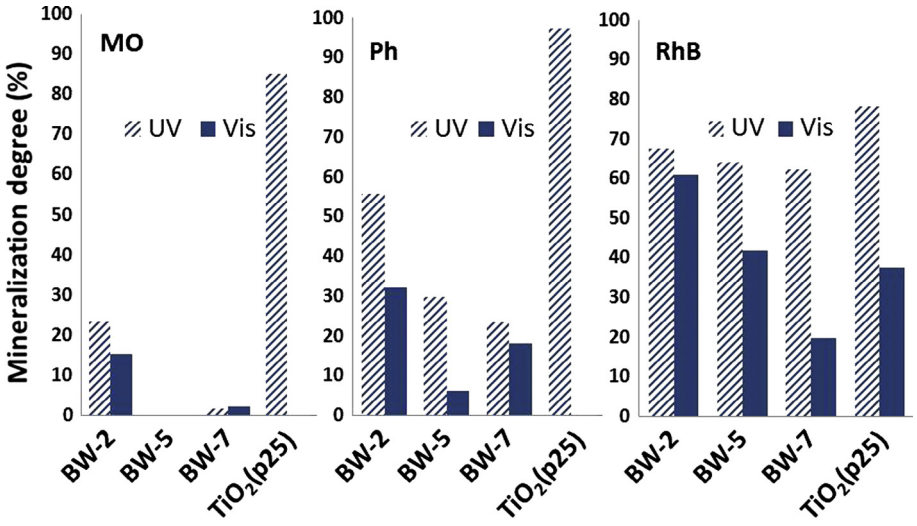

Figure 12 Mineralization degrees (%) calculated from the TOC final values (after 120 min) in the test using different photo-catalysts under both UV and sun-like illumination.

thing is the effectiveness, measured by the degree of mineralization obtained, one could conclude, based on the results of mineralization obtained with Rhodamine B, that the best of the three synthesized photo-catalysts is the BW-2, with both lighting conditions in the UV and in the visible.

Thus, focusing on the comparative results between the synthesized catalysts, when RhB is used as a substrate model, studying both values of initial reaction rates per unit area (Figs. 10 and 11) as well as the percentages of mineralization (Fig. 12), we can conclude there is a marked dependence on the pH value used in the synthesis of Bi_2WO_6 photo-catalysts. Thus, both in the UV and in the visible region of illumination, an increase in pH of synthesis leads to increased values of normalized initial rates per unit area and to a decrease in mineralization percentages. These results are associated in part with the values of specific surfaces of the samples and with the mechanism of photo-sensitization of RhB, this is, an increase in the specific surface of the photo-catalysts favors adsorption of RhB and consequently improves the mechanism of photo-sensitization associated with the substrate RhB. In fact, during the dark step, prior to illumination (20 min in the dark), the amounts of each substrates adsorbed on the surface of the three BW-x samples, were measured. Fig. 13 shows the percentages of the absorbed amounts, of each substrate, per surface area unit, of each photo-catalyst. As can be seen, the percentage of the amount of RhB adsorbed on the BW-7 sample is superior to those for the other substrates, BW-2, BW-5 and for TiO_2(P25, Evonik) samples.

One might think that, with MO being a dye, improvements by photo-sensitization mechanism associated with this dye could also be obtained. However, the results obtained for the three catalysts synthesized, when the MO is used, lead to think that the expected photo-sensitization mechanism of MO is not given (or given to a lesser extension), probably by the relative low adsorption interaction of MO on the surface of the synthesized catalysts if it is compared with the adsorption capability of RhB (Fig. 13).

The photo-catalytic properties of the BW-7 synthesized catalyst have been evaluated by exposing a mixture of RhB

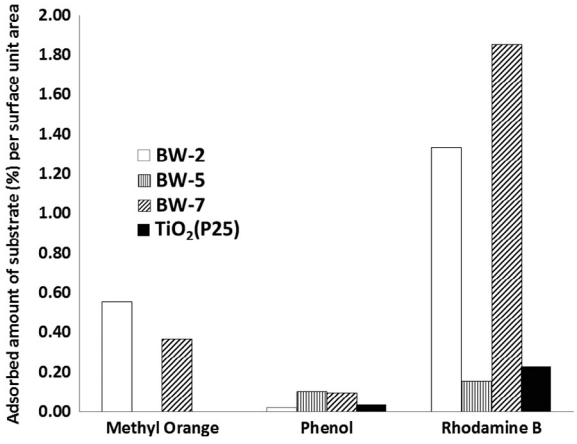

Figure 13 Adsorbed amount of the three choosed substrates (%) per surface area unit using the different catalysts. Data are obtained after 20 min in the dark.

(10 ppm) and Phenol (50 ppm) in water, to different illumination conditions. Fig. 14, shows the RhB and Phenol conversion plots in mixed solution of both substrates using BW-7 under UV-illumination, whereas in Fig. 15 the conversion plots under visible illumination are reported. It is noticeable to remark that, in mixed solutions there is a decrease in RhB conversion with respect to those obtained in single solutions, whereas Phenol remains almost unaffected in mixed solutions under both UV and visible illumination. In fact, observing the initial reaction rates (inserted in Figs. 14 and 15), it can be seen that there is a drastic decrease in the initial reaction rate of RhB conversion when it is in mixture with respect to the value obtained when it is as single substrate. It is curious to note that while the initial reaction rate of Phenol as single substrate is less influenced by the simultaneous presence of RhB under both illumination conditions, the conversion of RhB seems to be affected by the simultaneous presence of Phenol. This fact could be associated with a competition for adsorption centers between Phenol and Rhodamine B, inhibiting

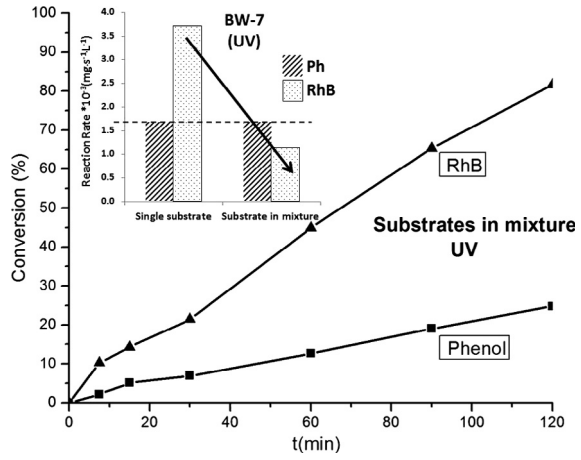

Figure 14 Rhodamine B (RhB) and Phenol (Ph) conversion plots in mixed solution with BW-7 under UV-illumination. Inserted, are reported the initial reaction rates for (Ph) or (RhB), single or mixture of both, using BW-7 catalyst under UV-illumination.

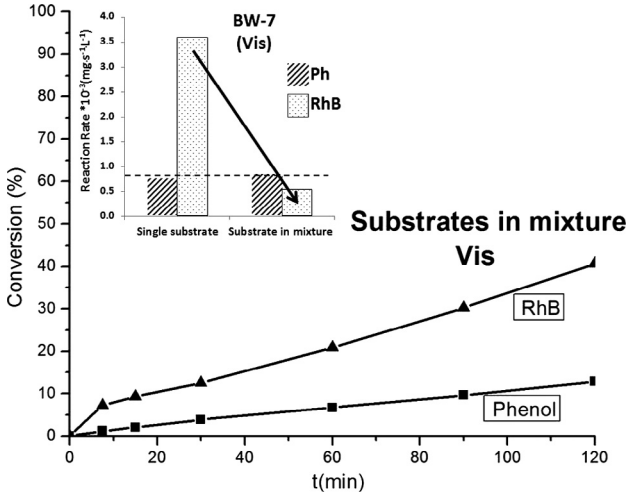

Figure 15 Rhodamine B (RhB) and Phenol (Ph) conversion plots in mixed solution with BW-7 under sun-like illumination. Inserted, are reported the initial reaction rates for (Ph) or (RhB), single or mixture of both, using BW-7 catalyst under sun-like illumination.

to some extent the photo-sensitizing effect of Rhodamine B. On the other hand, although our results, evidence the indicated fact, another reasonable explanation would require solid fundamentals before to propose a mechanism. However, a possible explanation could be that the intermediates of phenol degradation could retard the degradation of RhB degradation intermediates. The predominance of the N-deethylated or the direct chromophore cleavage mechanism for RhB degradation, depends both on the material and on the kind of illumination. Moreover, as we also concluded in our previous work (Murcia López et al., 2011), both occur under UV-vis light and almost no direct rupture takes place under only visible illumination.

In our previous work regarding TiO_2 incorporation into BW-2, the photo-catalytic activities were tested over single RhB (Colon et al., 2010) concluding that whether only RhB is used TiO_2 incorporation improves the BW-2 performance under both illumination conditions. When the activities are evaluated on Phenol photo-assisted degradation a completely different conclusion was established. When RhB/Phenol mixtures are used to determine whether TiO_2 incorporation has a positive or negative effect, it was proven that a photo-sensitizing molecule as RhB has some effect in the photo-degradation of a non-photo-sensitizing one, such as Phenol (Murcia-López et al., 2013a). However, in the present work, we use a selected photo-catalyst, BW-7 and when RhB/Phenol mixtures are used to determine whether a photo-sensitizing molecule has a positive effect in the photo-degradation of Phenol, we found that Phenol dramatically diminishes the conversion of RhB.

Based on the above results, it becomes obvious that evaluation of the photo-catalytic properties of a synthesized photo-catalyst deeply depends on the selected substrate. Thus, for instance, the photo-catalytic activity of most synthesized Bi_2WO_6 materials, by different methods (Shang et al., 2008; Wu et al., 2016; Xu et al., 2009; Zhang and Zhu, 2005), have been evaluated using dyes, specifically Rhodamine B, under visible light illumination. In our opinion, in the light of the results obtained in the present work, we believe that the conclusion on the photo-catalytic efficiency of the prepared samples reported in references using Rhodamine B could be another whether it had been another substrate, different to Rhodamine B, for instance Phenol.

4. Conclusions

Bi_2WO_6 was synthesized via mild hydrothermal treatment over three selected pH values (pH = 2.0, pH = 5.0 and pH = 7.0), using NaOH as precipitating agent. The pH of synthesis has a remarkable effect not only on morphologies, crystal sizes and textural properties but also on surface structure composition. Although the pH of synthesis has a marked influence on morphology, the nature of the precipitating agent (NaOH or TEA) also influences the morphology and texture. The band gap of the synthesized Bi_2WO_6 ranges from 2.78 to 2.98 eV, indicating its potential optical absorption in the visible range. However, our findings leave record that the evaluation of photo-catalytic activity in the visible tested using Rhodamine B, leads to results that are significantly better than if Phenol is used. What is striking about our results, in the visible, is that when another dye such as MO is used, no photo-catalytic activity is evident in the visible.

TiO_2(P25, Evonik) under visible illumination clearly showed that RhB degradation can be carried out by a photo-sensitized mechanism, as has been probed in our previous work using a home-prepared TiO_2 (Murcia-López et al., 2013a).

In summary, and by following the conclusive remarks that dyes other than Methylene Blue should also be examined for their suitability as probe molecules, and regarding the issue of whether a dye is a suitable substrate to assess the activity of a photo-catalyst, our results provide new evidences to the question posed by several Authors (Barbero and Vione, 2016; Konstantinou and Albanis, 2004; Yan et al., 2006).

Acknowledgment

This work was supported by research fund from Project Ref. CTQ2015-64664-C2-2-P (MINECO/FEDER UE). Research services of CITIUS University of Seville are also acknowledged. We thank the University of Tolima for economic support in the studies commission of César Augusto Jaramillo Páez.

References

Abdel-Maksoud, Y., Imam, E., Ramadan, A., 2016. TiO_2 solar photocatalytic reactor systems: selection of reactor design for scale-up and commercialization—analytical review. Catalysts 6, 1–26.

Abrahams, I., Nowinski, J.L., Bruce, P.G., Gibson, V.C., 1993. The disordered structure of WO_2Cl_2: a powder diffraction study. J. Solid State Chem. 102, 140–145.

Amano, F., Nogami, K., Abe, R., Ohtani, B., 2008. Preparation and characterization of bismuth tungstate polycrystalline flake-ball particles for photocatalytic reactions. J. Phys. Chem. C 112, 9320–9326.

Amano, F., Nogami, K., Ohtani, B., 2009. Visible light-responsive bismuth tungstate photocatalysts: effects of hierarchical architecture on photocatalytic activity. J. Phys. Chem. C 113, 1536–1542.

Babu, V.J., Bhavatharini, R.S.R., Ramakrishna, S., 2014a. Electrospun BiOI nano/microtectonic plate-like structure synthesis and UV-light assisted photodegradation of ARS dye. RSC Adv. 4, 19251–19256.

Babu, V.J., Bhavatharini, R.S.R., Ramakrishna, S., 2014b. Bi_2O_3 and BiOCl electrospun nanosheets and morphology-dependent photocatalytic properties. RSC Adv. 4, 29957–29963.

Barbero, N., Vione, D., 2016. Why dyes should not be used to test the photocatalytic activity of semiconductor oxides. Environ. Sci. Technol. 50, 2130–2131.

Bortoluzzi, M., Evangelisti, C., Marchetti, F., Pampaloni, G., Piccinelli, F., Zacchini, S., 2016. Synthesis of a highly reactive form of WO_2Cl_2, its conversion into nanocrystalline monohydrated WO_3 and coordination compounds with tetramethylurea. Dalt. Trans. 45, 15342–15349.

Chunmei, G., Zhiyu, W., Zhongping, Y., Bo, Y., Bo, L., Xianping, F., Guodong, Q., 2009. Effect of pH values on photocatalytic properties of Bi_2WO_6 synthesized by hydrothermal method. J. Wuhan Univ. Technol. Sci. Ed. 24, 533–536.

Colon, G., Murcia Lopez, S., Hidalgo, M.C., Navio, J.A., 2010. Sunlight highly photoactive Bi_2WO_6-TiO_2 heterostructures for rhodamine B degradation. Chem. Commun. 46, 4809–4811.

Di Paola, A., García-López, E., Marcì, G., Palmisano, L., 2012. A survey of photocatalytic materials for environmental remediation. J. Hazard. Mater. 211–212, 3–29.

Fagan, R., McCormack, D.E., Dionysiou, D.D., Pillai, S.C., 2016. A review of solar and visible light active TiO_2 photocatalysis for treating bacteria, cyanotoxins and contaminants of emerging concern. Mater. Sci. Semicond. Process. 42, 2–14.

Hu, S.-P., Xu, C.-Y., Zhen, L., 2013. Solvothermal synthesis of Bi_2WO_6 hollow structures with excellent visible-light photocatalytic properties. Mater. Lett. 95, 117–120.

Jaramillo-Páez, C., Navío, J.A., Hidalgo, M.C., Bouziani, A., Azzouzi, M. El, 2017. Mixed α-Fe_2O_3/Bi_2WO_6 oxides for photoassisted hetero-Fenton degradation of Methyl Orange and Phenol. J. Photochem. Photobiol. A Chem. 332, 521–533.

Konstantinou, I.K., Albanis, T.A., 2004. TiO_2-assisted photocatalytic degradation of azo dyes in aqueous solution: Kinetic and mechanistic investigations: a review. Appl. Catal. B Environ. 49, 1–14.

Malato, S., Maldonado, M.I., Fernández-Ibáñez, P., Oller, I., Polo, I., Sánchez-Moreno, R., 2016. Decontamination and disinfection of water by solar photocatalysis: The pilot plants of the Plataforma Solar de Almeria. Mater. Sci. Semicond. Process. 42, 15–23.

Mohamed, R.M., McKinney, D.L., Sigmund, W.M., 2012. Enhanced nanocatalysts. Mater. Sci. Eng. R Rep. 73, 1–13.

Murcia-López, S., Hidalgo, M.C., Navío, J.A., 2013a. Degradation of Rhodamine B/phenol mixtures in water by sun-like excitation of a Bi_2WO_6-TiO_2 photocatalyst. Photochem. Photobiol. 89, 832–840.

Murcia-López, S., Navío, J.A., Hidalgo, M.C., 2013b. Role of activated carbon on the increased photocatalytic activity of AC/Bi_2WO_6 coupled materials. Appl. Catal. A Gen. 466, 51–59.

Murcia López, S., Hidalgo, M.C., Navío, J.A., Colón, G., 2011. Novel Bi_2WO_6-TiO_2 heterostructures for Rhodamine B degradation under sunlike irradiation. J. Hazard. Mater. 185, 1425–1434.

Nakata, K., Fujishima, A., 2012. TiO_2 photocatalysis: design and applications. J. Photochem. Photobiol. C Photochem. Rev. 13, 169–189.

Ohtani, B., 2014. Revisiting the fundamental physical chemistry in heterogeneous photocatalysis: its thermodynamics and kinetics. Phys. Chem. Chem. Phys. 16, 1788–1797.

Shaham-Waldmann, N., Paz, Y., 2016. Away from TiO_2: a critical minireview on the developing of new photocatalysts for degradation of contaminants in water. Mater. Sci. Semicond. Process. 42, 72–80.

Shang, M., Wang, W., Sun, S., Zhou, L., Zhang, L., 2008. Bi_2WO_6 nanocrystals with high photocatalytic activities under visible light. J. Phys. Chem. C 112, 10407–10411.

Wang, D., Zhen, Y., Xue, G., Fu, F., Liu, X., Li, D., 2013. Synthesis of mesoporous Bi_2WO_6 architectures and their gas sensitivity to ethanol. J. Mater. Chem. C 1, 4153–4162.

Wu, C.-H., Kuo, C.-Y., Wu, J.-T., Hsu, M.-J., Jhang, T.-J., 2016. Photodegradation of C.I. Reactive Red 2 in the Bi_2WO_6 system: the determination of surface characteristics and photocatalytic activities of Bi_2WO_6. React. Kinet. Mech. Catal. 117, 391–404.

Xu, C., Wei, X., Ren, Z., Wang, Y., Xu, G., Shen, G., Han, G., 2009. Solvothermal preparation of Bi_2WO_6 nanocrystals with improved visible light photocatalytic activity. Mater. Lett. 63, 2194–2197.

Yan, X., Ohno, T., Nishijima, K., Abe, R., Ohtani, B., 2006. Is methylene blue an appropriate substrate for a photocatalytic activity test? A study with visible-light responsive titania. Chem. Phys. Lett. 429, 606–610.

Yu, J., Xiong, J., Cheng, B., Yu, Y., Wang, J., 2005. Hydrothermal preparation and visible-light photocatalytic activity of Bi_2WO_6 powders. J. Solid State Chem. 178, 1968–1972.

Zhang, C., Zhu, Y., 2005. Synthesis of square Bi_2WO_6 nanoplates as high-activity visible-light-driven photocatalysts. Chem. Mater. 17, 3537–3545.

Zhang, L., Wang, H., Chen, Z., Wong, P.K., Liu, J., 2011. Bi_2WO_6 micro/nano-structures: synthesis, modifications and visible-light-driven photocatalytic applications. Appl. Catal. B Environ. 106, 1–13.

Zhang, L., Wang, W., Zhou, L., Xu, H., 2007. Bi_2WO_6 nano- and microstructures: shape control and associated visible-light-driven photocatalytic activities. Small 3, 1618–1625.